FRONTIERS OF PHYSICS

RESEARCH ARTICLE
Volume 21 / Issue 4 / 042202 / 2026

Edge burst in population dynamics with rock–paper–scissors interactions

Jinfeng Liang[1], Qionglin Dai[1,2,†], Haoxin Cheng[1], Haihong Li[1,2], Junzhong Yang[1,‡]

1 School of Physical Science and Technology, Beijing University of Posts and Telecommunications, Beijing 100876, China
2 Key Laboratory of Mathematics and Information Networks (Beijing University of Posts and Telecommunications), Ministry of Education, Beijing 100876, China
Corresponding authors. E-mail: †qldai@bupt.edu.cn, ‡jzyang@bupt.edu.cn
Received April 25, 2025; accepted June 27, 2025

ABSTRACT

Non-Hermitian systems have been extensively studied for their unique topological properties and dynamic behaviors. In this paper, we investigate the phenomenon of edge bursts in population dynamics with rock–paper–scissors interactions, focusing on the interplay between non-Hermitian effects and biomass dissipation dynamics. We demonstrate that edge bursts occur when the energy bands form two distinct closed loops that do not intersect the real axis. Our findings reveal that the presence of non-dissipated sites is crucial for the formation of edge bursts, as they act as reservoirs, sustaining solitons near the boundaries and facilitating biomass transport to the edges. This study provides new insights into the behavior of non-Hermitian systems with open boundaries and asymmetric interactions, contributing to a broader understanding of complex phenomena in such systems.

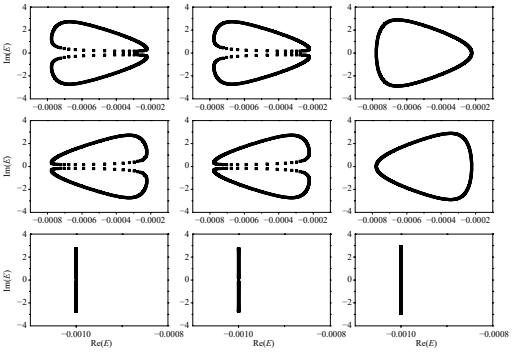

Keywords non-Hermitian, edge burst, population dynamics

1 Introduction

Non-Hermitian physics has emerged as a vibrant field of research, expanding our understanding of physical systems beyond the traditional Hermitian framework [1–3]. Unlike Hermitian systems, which are characterized by real eigenvalues and unitary evolution, non-Hermitian systems exhibit complex eigenvalues and have been found to possess unique topological properties. These properties are robust against perturbations and can be identified through topological order [4, 5]. Non-Hermitian skin effect (NHSE) is one of unique features of non-Hermitian systems under open boundary conditions (OBC), characterized by the localization of eigenstates near the boundaries of the system [6–11]. It represents a topological effect that can be seen as a manifestation of a truly non-Hermitian bulk-boundary correspondence [12–16]. NHSE highlights how boundary conditions and non-Hermitian properties can significantly influence the behavior of physical systems, leading to unique phenomena that are of great interest in both theoretical and experimental physics [17–20]. It has been observed in electronics and photonics systems, and non-Hermitian effects have also been reported in classical systems [21–24].

NHSE is recognized as a reflection of non-Hermitian static attributes. Recently, a dynamic phenomenon in a class of non-Hermitian systems has captured considerable interest [25–28]. Consider a quantum walker in a lossy lattice, an intriguing reversal occurs: an exceptionally large portion of loss occurs at the system boundary

*Special Topic: Non-Hermitian Physics (Eds.: Peng Xue, Lan Yang & Wu-Ming Liu).

Higher Education Press

https://doi.org/10.15302/frontphys.2026.042202

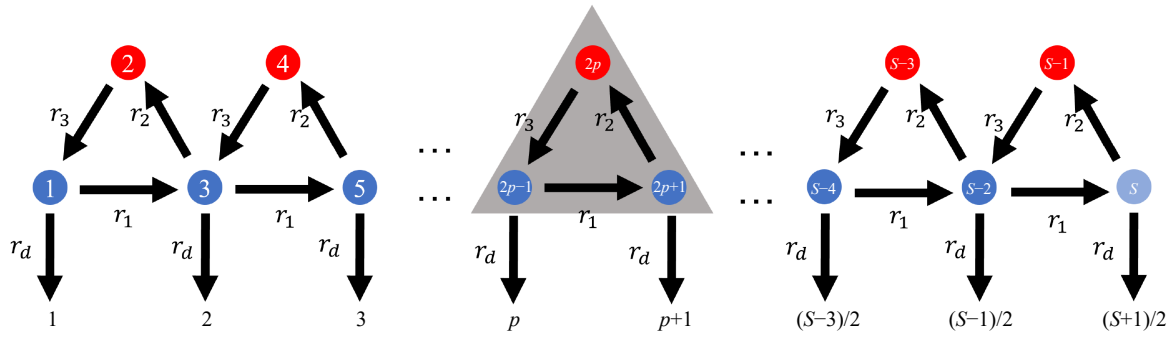

Fig. 1 Schematic diagram of a lossy chain composed of two-site cells for scenario A. Each cell p consists of sites $2p-1$ and $2p$, where p ranges from 1 to $\lfloor S/2 \rfloor$. The circled numbers represent site indices, and the numbers below indicate cell indices. Each triangle symbolizes a rock-paper-scissors interaction, with r_1 and r_2 denoting the inter-cell interaction strengths and r_3 representing the intra-cell interaction strength. The mortality rate r_d in the population dynamics signifies the dissipation. Under periodic boundary conditions, site S is equivalent to site 1.

rather than the initial position of the particle [26]. This stands in stark contrast to the conventional expectation of particle dissipation occurring predominantly at the initial location. This counterintuitive occurrence is labeled as edge burst.

Since both NHSE and edge burst involve boundary localization, one intuition is to attribute the latter to the former. However, Xue *et al.* [29] studied quantum-mechanical time evolution of quantum walkers in a lossy lattice. They differentiate edge bursts from NHSE and argued that the emergence of edge bursts arise from an unforeseen interaction between two distinct non-Hermitian phenomena: the non-Hermitian skin effect and imaginary gap closing. Wen *et al.* [30] investigated the evolution of real-space wave functions for this lossy lattice system. Using time-dependent perturbation theory, they derived the analytical expression of the real-space wave functions and found that wave function of the edge site is distinct from the bulk sites. Following this line of research, edge bursts have been experimentally observed by Zhu *et al.* [31] in a non-Hermitian Su–Schrieffer–Heeger (SSH) lattice with bulk translation symmetry, using a photonic quantum walk, and by Xiao *et al.* [32] using a discrete-time non-Hermitian quantum walker of photons. These studies collectively explore the traits and prerequisites of edge bursts in quantum systems. However, a quantum walker in a lattice corresponds to a diffusion problem. Whether these claims are applicable to other types of systems such as a drifting particle in a lossy lattice remains an open problem. Additionally, it is also pertinent to inquire whether edge bursts can be observed in classical systems under suitable conditions.

To date, non-Hermitian phenomena in classical systems, particularly in population dynamics, have also been observed and studied [33–35]. Building on this, we concentrate population dynamics on one-dimensional chains with rock–paper–scissors (RPS) interaction and examine the system's evolution under loss by incorporating the population's mortality rate. The RPS interaction breaks Hermiticity, leading to complex eigenvalues that enable topological phenomena like the NHSE, which is beyond Hermitian framework. After numerically simulating the mass evolution equation and witnessing the phenomena of edge bursts, we explore the microscopic mechanism behind edge bursts in this population dynamical system. Moreover, we develop an effective Hamiltonian and find that there is no clear relation between the band characteristics and edge bursts.

The remainder of this paper is structured as follows: Section 2 outlines the model. In Section 3, we firstly numerically demonstrate the presence of edge bursts and delve into the mechanism behind edge bursts. Then we explore the relation between the system's band characteristics and edge bursts via an effective Hamiltonian. Lastly, Section 4 offers a comprehensive summary.

2 Model

We consider an antisymmetric Lotka–Volterra equation (ALVE) [36] defined on a network with S sites (S is an odd number), which serves as the foundation for our investigation into the phenomenon of edge bursts within population dynamics. As depicted in Fig. 1, the network is structured as a one-dimensional chain of $n = \lfloor S/2 \rfloor$ two-site cells, where $\lfloor \cdot \rfloor$ denotes the floor function. For simplicity, we assume that cell p contains sites $2p-1$ and $2p$. Our system is subject to open boundary conditions (OBCs), with site 1 and site S serving as the boundaries of the system.

The biomass at each site i is denoted as x_i and evolves according to the coupled ordinary differential equations:

$$\frac{\mathrm{d}}{\mathrm{d}t}x_i = x_i \sum_{j=1}^{S} a_{ij}x_j - m_i x_i. \tag{1}$$

The first term on the right-hand side signifies the interaction between adjacent sites with a_{ij} representing the interaction strength between sites i and j for $j \neq i$. Assuming the interaction between sites following the RPS model, we impose the condition $a_{ij} = -a_{ji}$ and assign interaction strengths as follows: $a_{ij} = r_1$ if $i = 2p+1$ and $j = 2p-1$, $a_{ij} = r_2$ if $i = 2p$ and $j = 2p+1$, $a_{ij} = -r_3$ if $i = 2p$ and $j = 2p-1$ with $p = 1, 2, \cdots, n$, and $a_{ij} = 0$ otherwise. The parameters r_1, r_2, and r_3 are positive and account for the intra-cell and inter-cell interaction strengths, respectively. The second term in Eq. (1) introduces mortality at site i, which refers to the loss of the biomass at site i via the interaction with the environment, leading to the dissipation of biomass from site i. m_i is the dissipation rate of site i, which characterizes the interaction strength between site i and the environment. The condition $a_{ij} = -a_{ji}$ is the requirement of biomass conservation in the absence of dissipation rate in corresponding to lossless quantum walker in SSH model, and represents predator-prey interaction required by the maintenance of biodiversity in ecology. To be noted, the 1D RPS chain is the minimal topologically nontrivial system and serves as a classical analog of 1D SSH model. We consider three scenarios, scenario A with $m_{2p-1} = r_d$ and $m_{2p} = 0$, scenario B with $m_{2p-1} = 0$ and $m_{2p} = r_d$, and scenario C with $m_i = r_d$. In scenarios A and B, each cell contains only one dissipated site. To be noted, in scenario C, the total biomass decays exponentially with the exponent r_d, which is not satisfied in scenarios A and B.

In essence, our model captures the dynamics of a population with RPS interactions under the influence of dissipation, offering a framework to explore the emergence of edge bursts. For this aim, we establish specific initial conditions with biomass concentrated at an initial position i_0 (aggregated biomass), for example $x_{i_0} = 0.99$ and the biomass of 0.01 is uniformly distributed onto all other sites (distributed biomass). Intuitively, it is expected that the majority of biomass should be dissipated around i_0. However, our findings will reveal that, contrary to the expectation, biomass dissipation tends to accumulate at the system's boundary. In the following, we let $S = 61$ and $i_0 = 45$.

3 Results

3.1 Numerical results on population dynamics

In our previous work, we delved into the population dynamics of model (1) in the absence of dissipation ($r_d = 0$) [35]. We discovered that the right edge state, characterized by biomass localizing at the right edge, occurred when $r_2 < r_3$, and the left edge state occurred when $r_2 > r_3$, irrespective of r_1. In this study, we set $r_1 = 0.8$ and explore the biomass dissipation dynamics with non-zero r_d. We focus on the dependence of biomass dissipation on the dissipation rate r_d and the edge states, as well as the mechanism underlying the edge burst. To achieve this, we numerically simulate model (1) using the fourth-order Runge–Kutta algorithm with a time step of 0.01. To extract information on biomass dissipation, we monitor the accumulated dissipated biomass on all sites, defined as $\eta_i = \int_0^T m_i x_i \mathrm{d}t$ for each site i, up to a specified time T. Additionally, we monitor the remaining biomass $x_i(t)$ for each site i and the total remaining biomass $X(t) = \sum_i x_i(t)$.

We commence our investigation with scenario A, where $m_{2p-1} = r_d$ and $m_{2p} = 0$. Figure 2 illustrates the relationship between edge bursts and edge states, as well as the dissipation rate, with $T = 30\,000$. At a low dissipation rate, such as $r_d = 10^{-4}$, edge bursts are strongly correlated with edge states. For instance, in Fig. 2(a1), with $r_2 = 1.2$ and $r_3 = 1$, the left edge state is present, and η_i exponentially decreases with distance from the left edge. Conversely, in Fig. 2(a2), with $r_2 = 1$ and $r_3 = 1.2$, the right edge state is present, and η_i exhibits an exponential decay with distance from the right edge. Notably, when $r_2 = r_3$ and no edge state exists, as shown in Fig. 2(a3), no edge bursts are observed. The inset in Fig. 2(a2) indicates that the total biomass in the lattice decreases exponentially over time.

Upon increasing r_d to 10^{-3}, the correlation between edge bursts and edge states remain consistent, as seen in Figs. 2(b1)–(b3). The effect of the dissipation rate is evident in the interruption of the exponential decay of accumulated dissipated biomass by a plateau in the system's central region. At a higher dissipation rate of $r_d = 0.01$, Figs. 2(c1)–(c3) show the disappearance of edge bursts regardless of the combination of r_2 and r_3. Instead, the dissipated biomass accumulates in the middle domain on the right side of the initial biomass concentration i_0. It is important to note that the insets in Figs. 2(b2) and (c2) indicate a decrease in remaining biomass in the lattice that is slower than exponential.

The insets in Figs. 2(c1) and (c3) summarize the impacts of the dissipation rate on edge bursts. In the inset of Fig. 2(c1), the ratio η_1/η_{i_0} is plotted against the dissipation rate r_d at the same combination of r_2 and r_3, where η_1 represents the dissipated biomass at the left edge and η_{i_0} is the dissipated biomass at initial position. The results show that there is a threshold r_d^* beyond which edge bursts are lost (i.e., $\eta_1/\eta_{i_0} < 1$). In the inset of Fig. 2(c3), the threshold r_d^* is presented as a function of r_3. It can be seen that r_d^* against r_2 is discontinuous at $r_3 = r_2$, revealing the strong correlation between edge bursts and the existence of edge states. Additionally, this indicates that the edge burst at the left edge is more robust than that at the the right edge.

Next, we explore the development of edge bursts. Taking $r_d = 10^{-3}$ as an example, for $r_2 = 1.2$ and $r_3 = 1$, the spatial-temporal plots of the biomass and the accumulated dissipated biomass are shown in Figs. 3(a1) and

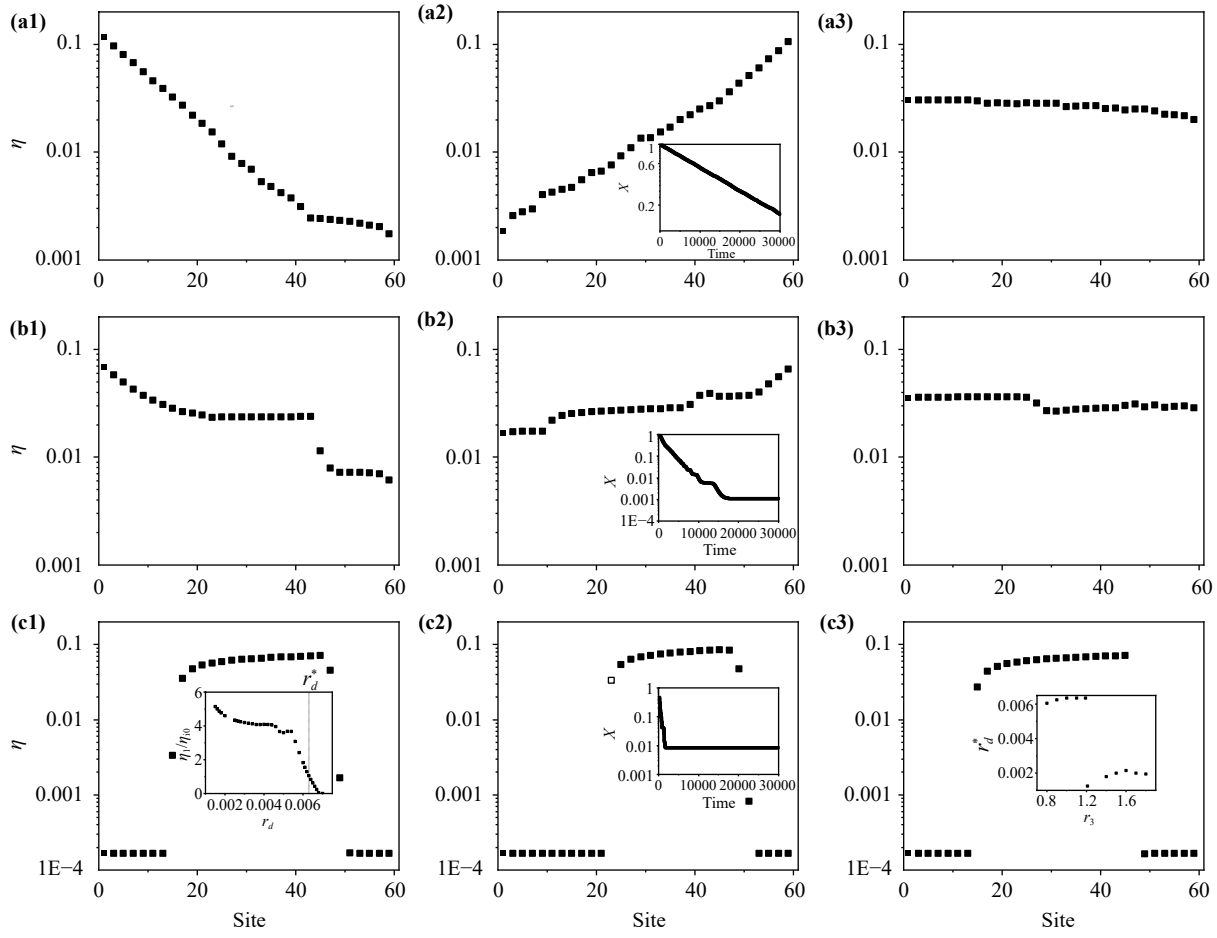

Fig. 2 The accumulated dissipated biomass distribution η for the ALVE model in scenario A under various parameter settings. The dissipation rate r_d is set to 10^{-4} in the top panels **(a1–a3)**, 10^{-3} in the middle panels **(b1–b3)**, and 10^{-2} in the bottom panels **(c1–c3)**. The interaction parameters are as follows: $r_2 = 1.2$ and $r_3 = 1$ in the left column, $r_2 = 1$ and $r_3 = 1.2$ in the middle column, and $r_2 = 1.2$ and $r_3 = 1.2$ in the right column. The insets in the middle column display the evolution of the total remaining biomass, $X(t)$, in the system. The inset of (c1) displays the ratio η_1/η_{i_0} against r_d. Beyond the threshold r_d^*, edge bursts are lost. The inset of (c3) presents r_d^* against r_3 at $r_2 = 1.2$ where the discontinuity at $r_3 = 1.2$ suggests the correlation between edge bursts and edge states. Other parameters: $S = 61$, $i_0 = 45$, $r_1 = 0.8$, and $T = 30\,000$.

(a2). We define aggregated biomass as the biomass initially concentrated at site i_0, which behaves like dissipative solitons, and distributed biomass as the biomass spread across the rest of the system. For $i_0 = 45$, aggregated biomass, resulting from the RPS interaction, splits into two solitons, a large one propagating leftwards and a small one propagating rightwards. The large soliton travels a significantly longer distance, reversing its direction from rightward to leftward after bouncing back from the left boundary. In contrast, the small soliton dissipates before reaching the right boundary. Both solitons experience a biomass loss to the surrounding distributed biomass or the environment, with a notable loss of approximately one order of magnitude within the first 100 time units. This loss is indicative of the solitons' interaction with the environment and their gradual dissolution into the distributed biomass. To be noted, the propagating velocities of solitons are positively correlated with their carried biomass.

Without the disturbance of solitons, the distributed biomass exhibits a homogeneous distribution across cells, with biomass on dissipated sites being depleted and non-dissipated sites maintaining higher levels. The passage of solitons through the system causes a jump in the biomass level on subsequent sites, demonstrating the solitons' gradual dissolution. Remarkably, the distributed biomass generates a cascade of traveling waves that transport biomass to the left edge. These waves are initiated from non-dissipated sites that are initially close to the left edge and gradually move further away from it. The spatiotemporal plot of accumulated dissipated biomass in Fig. 3(a2) shows that passing solitons induce a jump in the accumulated dissipated biomass. However, the development of edge bursts at left edge is facilitated by the traveling waves from the distributed biomass. In short, the solitons are instrumental

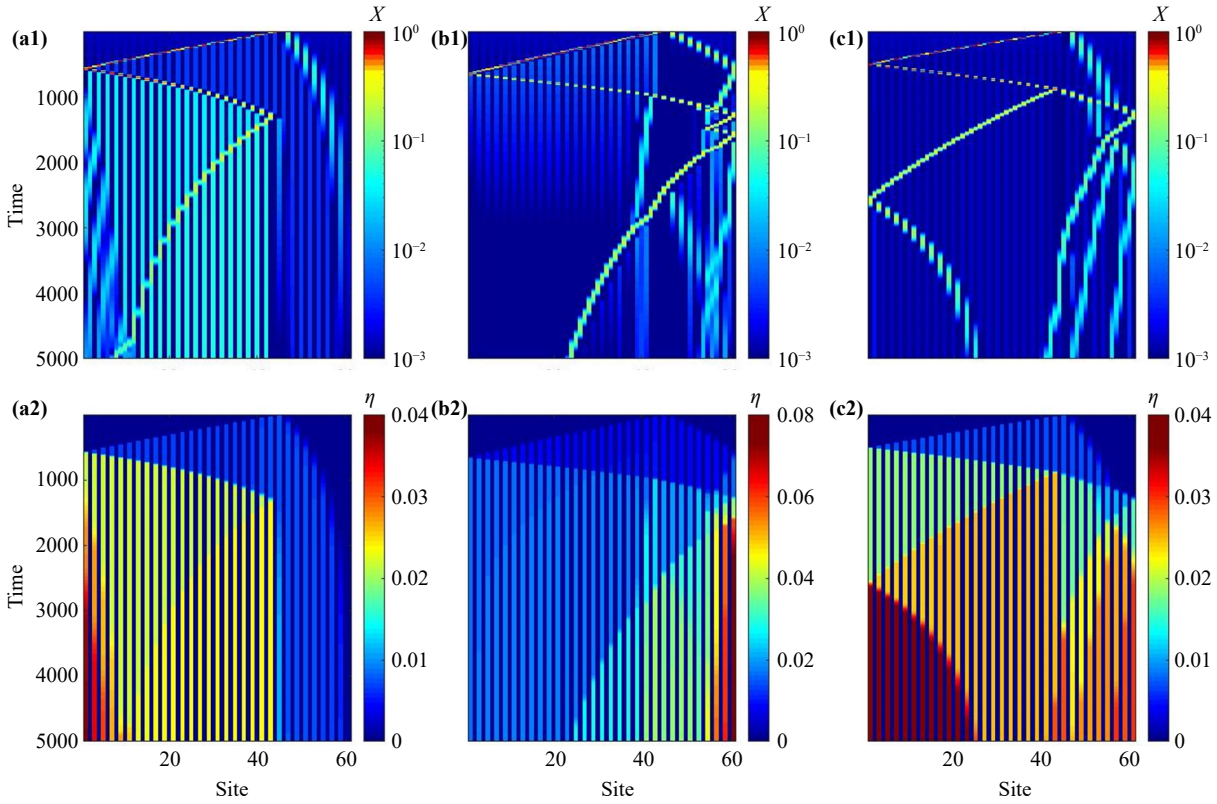

Fig. 3 The spatial-temporal evolution of the biomass $x_i(t)$ (top panels) and the accumulated dissipated biomass $\eta_i(t)$ (bottom panels) for scenario A. The left column corresponds to $r_2 = 1.2$ and $r_3 = 1$, the middle column to $r_2 = 1$ and $r_3 = 1.2$, and the right column to $r_2 = 1.2$ and $r_3 = 1.2$. Other parameters: $r_d = 10^{-3}$, $S = 61$, $i_0 = 45$, and $r_1 = 0.8$.

in the formation of edge bursts by dispersing the initial aggregated biomass into the distributed biomass through their motion. This dynamic interplay between the solitons and the distributed biomass is responsible for the observed biomass dissipation at the left edge of the system.

Figures 3(b1) and (b2) illustrate the distinct characteristics of edge bursts at the right edge compared to those at the left edge, under conditions where $r_2 = 1$ and $r_3 = 1.2$. Notably, the small soliton, carrying a larger biomass, predominantly resides near the right edge. In contrast, the large soliton swiftly moves to the right edge after rebounding from the left, lingering there before eventually moving away. These behaviors result in increased biomass available to be dissipated at the right edge. Conversely, the contribution of distributed biomass transportation to edge bursts, which is evident on the left, is diminished due to RPS interactions. Additionally, the accumulation of dissipated biomass indicates that right-edge bursts develop more rapidly than their left-edge counterparts. These findings highlight that, though the phenomena of edge bursts are similar, the underlying dynamics differ significantly between the left and right edges. Figures 3(c1) and (c2) present the scenario where $r_2 = 1.2$ and $r_3 = 1.2$, with no observable edge bursts. Despite the non-uniform distribution of dissipated biomass, no distinct edge bursts are evident at either edge. This is attributed to solitons near the edges having already dispersed a significant portion of biomass during their transit through the central region. The presence of non-dissipated sites is crucial for edge bursts, as they serve as biomass reservoirs that sustain solitons near the boundaries and support leftward-propagating traveling waves, ultimately leading to edge bursts.

In our final numerical exploration, we examine edge bursts in scenario B, with $m_{2p} = r_d$ and $m_{2p-1} = 0$, and in scenario C, with $m_i = r_d$, setting $r_d = 10^{-4}$. As depicted in Fig. 4, edge bursts are observed in scenario B, aligning with the expected correspondence between edge state and edge bursts occurrence, which is not the case in scenario C. The lack of edge bursts in scenario C underscores the significance of non-dissipated sites in facilitating edge bursts. In the absence of non-dissipated sites acting as mass reservoirs, the traveling waves critical for the left edge case and the prolonged presence of solitons near the edges are suppressed, thereby inhibiting the occurrence of edge bursts.

3.2 Energy spectrum of non-Hermitian systems

Our numerical findings have established that the presence

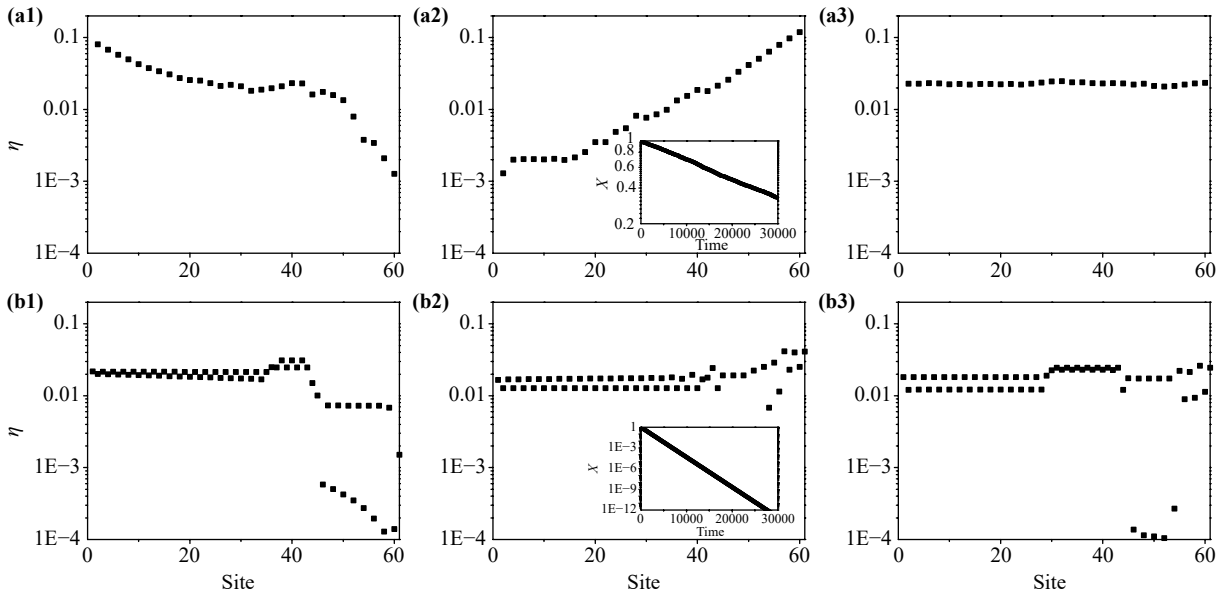

Fig. 4 Accumulated dissipated biomass distribution η for the ALVE model in scenario B (top panels) and scenario C (bottom panels). The left column corresponds to $r_2 = 1.2$ and $r_3 = 1$, the middle column to $r_2 = 1$ and $r_3 = 1.2$, and the right column to $r_2 = 1.2$ and $r_3 = 1.2$. The insets in the middle column display the evolution of the total remaining biomass, $X(t)$, in the system. Other parameters: $r_d = 10^{-4}$, $S = 61$, $i_0 = 45$, $r_1 = 0.8$, and $T = 30\,000$.

of edge states in the absence of dissipation is essential for the occurrence of edge bursts. We now investigate the band characteristics associated with edge bursts in the ALVE system. As in Ref. [35], we define creation and annihilation operators $a_i^\dagger$, a_i (for site $2i-1$) and $b_i^\dagger$, b_i (for site $2i$). The number operators $a_i^\dagger a_i$ and $b_i^\dagger b_i$ represent the number of individuals at sites $2i-1$ and $2i$, respectively. Using these operators, the predation processes in Eq. (1) can be reformulated. For instance, the predation between sites $2i-1$ and $2i$ is represented by $r_3 a_i^\dagger b_i$ (predation of site $2i$ by site $2i-1$ with strength r_3) and $-r_3 b_i^\dagger a_i$ (predation of site $2i-1$ by site $2i$ with the same strength). Consequently, we construct an effective Hamiltonian for a chain of two-site cells with periodic boundary conditions, corresponding to Eq. (1):

$$\begin{aligned}\hat{H} = \sum_i^n (&r_3 a_i^\dagger b_i - r_3 b_i^\dagger a_i + r_1 a_{i-1}^\dagger a_i - r_1 a_{i+1}^\dagger a_i \\ &+ r_2 a_{i+1}^\dagger b_i - r_2 b_{i-1}^\dagger a_i - m a_i^\dagger a_i - m' b_i^\dagger b_i)\end{aligned} \tag{2}$$

with the boundary condition $a_{n+1} = a_1$. The terms $-m a_i^\dagger a_i$ and $-m' b_i^\dagger b_i$ represent the dissipations at sites $2i-1$ and $2i$, respectively. $m = r_d$ and $m' = 0$ for scenario A, $m = 0$ and $m' = r_d$ for scenario B, and $m = m' = r_d$ for scenario C. We further introduce annihilation operators $\widetilde{a}_k$ and $\widetilde{b}_k$ such that $a_i = \frac{1}{\sqrt{n}} \sum_k \widetilde{a}_k \mathrm{e}^{-\mathrm{j}ki}$ and $b_i = \frac{1}{\sqrt{n}} \sum_k \widetilde{b}_k \mathrm{e}^{-\mathrm{j}ki}$ with j being the imaginary unit and $k = \frac{2\pi}{n} i$ $(i = 1, \cdots, n)$. The Hamiltonian (2) is then reformulated as

$$\begin{aligned} H &= \sum_k (r_3 \widetilde{a}_k^\dagger \widetilde{b}_k - r_3 \widetilde{b}_k^\dagger \widetilde{a}_k + r_1 \widetilde{a}_k^\dagger \widetilde{a}_k \mathrm{e}^{-\mathrm{j}k} - r_1 \widetilde{a}_k^\dagger \widetilde{a}_k \mathrm{e}^{\mathrm{j}k} \\ &\quad + r_2 \widetilde{a}_k^\dagger \widetilde{b}_k \mathrm{e}^{\mathrm{j}k} - r_2 \widetilde{b}_k^\dagger \widetilde{a}_k \mathrm{e}^{-\mathrm{j}k} - m \widetilde{a}_k^\dagger \widetilde{a}_k - m' \widetilde{b}_k^\dagger \widetilde{b}_k) \\ &= \sum_k (\widetilde{a}_k^\dagger, \widetilde{b}_k^\dagger) \widetilde{H}(k) (\widetilde{a}_k, \widetilde{b}_k)^{\mathrm{T}}, \end{aligned} \tag{3}$$

with the Bloch Hamiltonian

$$\widetilde{H}(k) = \begin{pmatrix} r_1(\mathrm{e}^{-\mathrm{j}k} - \mathrm{e}^{\mathrm{j}k}) - m & r_3 - r_2 \mathrm{e}^{-\mathrm{j}k} \\ -r_3 + r_2 \mathrm{e}^{\mathrm{j}k} & -m' \end{pmatrix}. \tag{4}$$

For each value of k, the Bloch Hamiltonian $\widetilde{H}(k)$ yields two eigenvalues, $E^{\pm}(k)$, which delineate two distinct energy bands as k ranges from 0 to 2π. The Bloch energy spectra for scenarios A, B, and C are depicted in Fig. 5. Contrary to the common assumption that edge bursts occur when the Bloch energy spectrum touches the real axis (indicating imaginary gap closing), we find that edge bursts actually occur only when the two energy bands form two distinct, closed loops that do not intersect the real axis. When the energy bands form a single closed loop that crosses the real axis, no edge bursts are observed. Furthermore, the mere presence of two separated energy bands does not ensure edge bursts, as edge bursts do not occur when the spectra for scenario C consist of two distinct line segments.

4 Conclusion

In this work, we have explored the phenomenon of edge

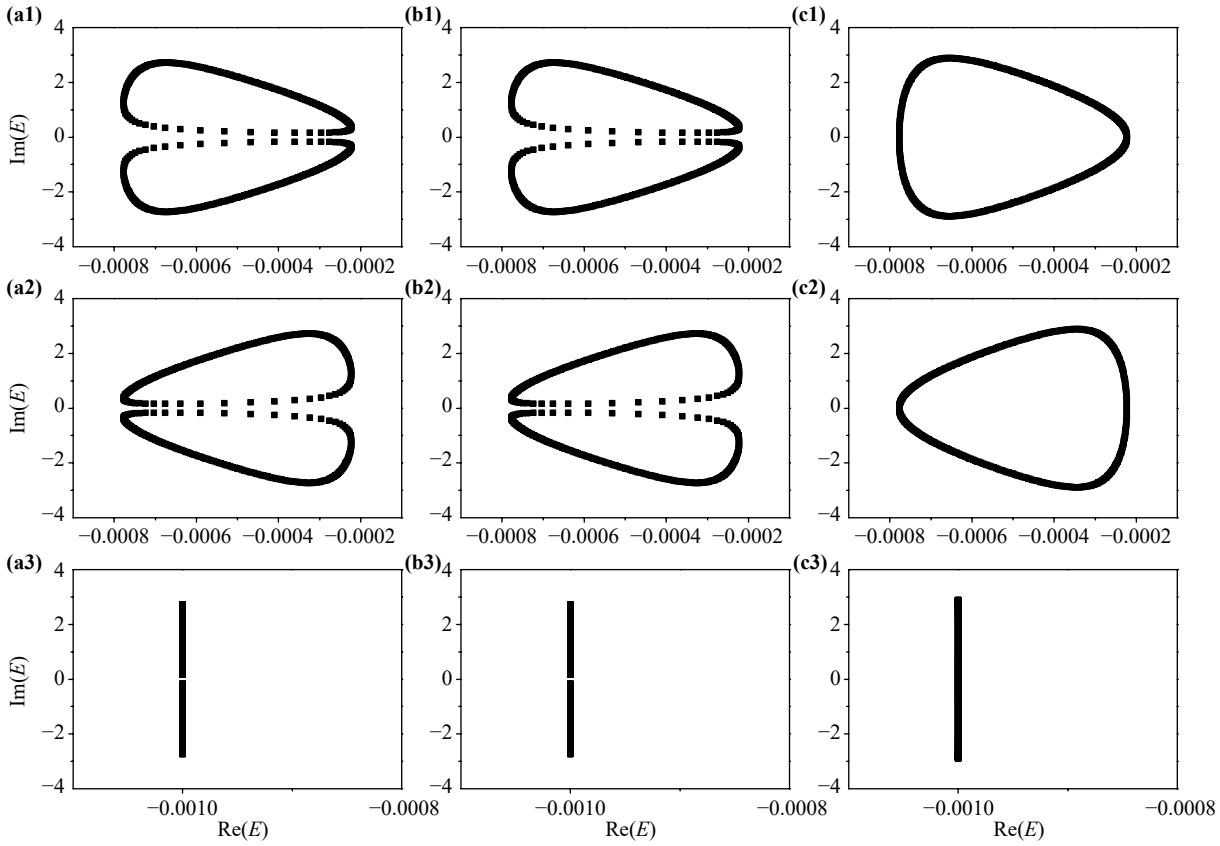

Fig. 5 Energy spectra under periodic boundary conditions for scenario A (top panels), scenario B (middle panels), and scenario C (bottom panels). The left column corresponds to $r_2 = 1.2$ and $r_3 = 1$, the middle column to $r_2 = 1$ and $r_3 = 1.2$, and the right column to $r_2 = 1.2$ and $r_3 = 1.2$. Other parameters: $r_d = 10^{-3}$, $S = 200$, and $r_1 = 0.8$.

bursts in population dynamics with rock–paper–scissors interactions, focusing on the interplay between non-Hermitian effects and the unique dynamics of biomass distribution. Our primary findings reveal that edge bursts are not solely a manifestation of the non-Hermitian skin effect, as previously thought. Instead, they arise from a complex interplay between the non-Hermitian skin effect and the dynamics of biomass dissipation, particularly in systems with asymmetric interactions. We have demonstrated that edge bursts occur when the energy bands form two distinct closed loops that do not intersect the real axis. This differs from the typical belief that edge bursts are linked to the closing of imaginary gaps, thereby emphasizing the need to consider both topological and dynamic aspects in ALVE. Furthermore, our investigation of the ALVE model has shown that the presence of non-dissipated sites is crucial for the formation of edge bursts. These sites act as reservoirs, sustaining solitons near the boundaries and facilitating the transport of biomass to the edges. This insight underscores the role of system architecture and boundary conditions in influencing the emergence of complex phenomena in non-Hermitian systems.

For physical implications, this work establishes edge bursts as a universal non-Hermitian phenomenon transcending quantum-classical boundaries. We observe the same edge burst, originally predicted in quantum walks, in classical population systems, confirming non-Hermitian topology as a cross-scale principle. Moreover, edge bursts in this work emerge from dynamic synergy of NHSE and dissipation, contrasting prior static localization studies. This enables ALVE to serve as a minimal laboratory for testing non-Hermitian quantum-classical correspondence. For ecological implications, this work predicts a phenomenon of boundary-driven extinction where high mortality at habitat edges occurs even when threats (e.g., pollutants) originate centrally. It also provides a quantifiable design rule for reserves where non-dissipative sites (e.g., protected core zones) sustain biomass reservoirs. Furthermore, the critical dissipation rate for edge bursts signals proximity to ecosystem tipping points, enabling proactive intervention.

Additionally, since both Fig. 1 and the Hamiltonian (2) suggest that model (1) is a classical analog of the 1D non-Hermitian SSH model, the predicted edge burst phenomenon may be observed experimentally in photonic quantum walks, either via a cascaded interferometer network [32] or a fiber-optic loop [31]. Furthermore, because RPS interactions have been reported for a system of bacteria [37], and human societies [38], we also

expect the observation of edge bursts in such systems. These platforms bridge quantum-inspired topology and classical dynamics, enabling direct observation of the interplay between non-Hermitian skin effects and dissipation-driven edge bursts.

Declarations The authors declare that they have no competing interests and there are no conflicts.

References

1. K. Kawabata, K. Shiozaki, M. Ueda, and M. Sato, Symmetry and topology in non-Hermitian physics, *Phys. Rev. X* 9(4), 041015 (2019)
2. Y. Ashida, Z. Gong, and M. Ueda, Non-Hermitian physics, *Adv. Phys.* 69(3), 249 (2020)
3. E. J. Bergholtz, J. C. Budich, and F. K. Kunst, Exceptional topology of non-Hermitian systems, *Rev. Mod. Phys.* 93(1), 015005 (2021)
4. X. Li, J. Liu, and T. Liu, Localization-delocalization transitions in non-Hermitian Aharonov–Bohm cages, *Front. Phys. (Beijing)* 19(3), 33211 (2024)
5. Y. Zou, Y. Zhou, L. Chen, and P. Ye, Detecting bulk and edge exceptional points in non-Hermitian systems through generalized Petermann factors, *Front. Phys. (Beijing)* 19(2), 23201 (2024)
6. S. Yao and Z. Wang, Edge states and topological invariants of non-Hermitian systems, *Phys. Rev. Lett.* 121(8), 086803 (2018)
7. V. M. Martinez Alvarez, J. E. Barrios Vargas, and L. E. F. Foa Torres, Non-Hermitian robust edge states in one dimension: Anomalous localization and eigenspace condensation at exceptional points, *Phys. Rev. B* 97, 121401(R) (2018)
8. C. H. Lee and R. Thomale, Anatomy of skin modes and topology in non-Hermitian systems, *Phys. Rev. B* 99, 201103(R) (2019)
9. L. Li, C. H. Lee, S. Mu, and J. Gong, Critical non-Hermitian skin effect, *Nat. Commun.* 11(1), 5491 (2020)
10. K. Zhang, Z. Yang, and C. Fang, Universal non-Hermitian skin effect in two and higher dimensions, *Nat. Commun.* 13(1), 2496 (2022)
11. R. Lin, T. Tai, L. Li, and C. Lee, Topological non-Hermitian skin effect, *Front. Phys. (Beijing)* 18(5), 53605 (2023)
12. T. E. Lee, Anomalous edge state in a non-Hermitian lattice, *Phys. Rev. Lett.* 116(13), 133903 (2016)
13. F. K. Kunst, E. Edvardsson, J. C. Budich, and E. J. Bergholtz, Biorthogonal bulk–boundary correspondence in non-Hermitian systems, *Phys. Rev. Lett.* 121(2), 026808 (2018)
14. K. Yokomizo and S. Murakami, Non-Bloch band theory of non-Hermitian systems, *Phys. Rev. Lett.* 123(6), 066404 (2019)
15. Z. Yang, K. Zhang, C. Fang, and J. Hu, Non-Hermitian bulk–boundary correspondence and auxiliary generalized Brillouin zone theory, *Phys. Rev. Lett.* 125(22), 226402 (2020)
16. T. Helbig, T. Hofmann, S. Imhof, M. Abdelghany, T. Kiessling, L. W. Molenkamp, C. H. Lee, A. Szameit, M. Greiter, and R. Thomale, Generalized bulk–boundary correspondence in non-Hermitian topolectrical circuits, *Nat. Phys.* 16(7), 747 (2020)
17. R. Y. Zhang, X. Cui, W. J. Chen, Z. Q. Zhang, and C. T. Chan, Symmetry-protected topological exceptional chains in non-Hermitian crystals, *Commun. Phys.* 6(1), 169 (2023)
18. S. Weidemann, C. Leefmans, M. C. Rechtsman, and A. Szameit, Topological triple phase transition in non-Hermitian Floquet quasicrystals, *Nature* 601, 354 (2022)
19. J. W. Ryu, J. H. Han, C. H. Yi, M. J. Park, and H. C. Park, Exceptional classifications of non-Hermitian systems, *Commun. Phys.* 7(1), 109 (2024)
20. Z. Li, L. W. Wang, X. Wang, Z. K. Lin, G. Ma, and J. H. Jiang, Observation of dynamic non-Hermitian skin effects, *Nat. Commun.* 15(1), 6544 (2024)
21. L. Zhang, Y. Yang, Y. Ge, Y. J. Guan, Q. Chen, Q. Yan, F. Chen, R. Xi, Y. Li, D. Jia, S. Q. Yuan, H. X. Sun, H. Chen, and B. Zhang, Acoustic non-Hermitian skin effect from twisted winding topology, *Nat. Commun.* 12(1), 6297 (2021)
22. T. Yoshida and Y. Hatsugai, Bulk-edge correspondence of classical diffusion phenomena, *Sci. Rep.* 11(1), 888 (2021)
23. E. Martello, Y. Singhal, B. Gadway, T. Ozawa, and H. M. Price, Coexistence of stable and unstable population dynamics in a nonlinear non-Hermitian mechanical dimer, *Phys. Rev. E* 107(6), 064211 (2023)
24. M. Reisenbauer, H. Rudolph, L. Egyed, K. Hornberger, A. V. Zasedatelev, M. Abuzarli, B. A. Stickler, and U. Delić, Non-Hermitian dynamics and non-reciprocity of optically coupled nanoparticles, *Nat. Phys.* 20(10), 1629 (2024)
25. M. S. Rudner, and L. S. Levitov, Topological transition in a non-Hermitian quantum walk, *Phys. Rev. Lett.* 102(6), 065703 (2009)
26. L. Wang, Q. Liu, and Y. Zhang, Quantum dynamics on a lossy non-Hermitian lattice, *Chin. Phys. B* 30(2), 020506 (2021)
27. H. Li and S. Wan, Dynamic skin effects in non-Hermitian systems, *Phys. Rev. B* 106(24), L241112 (2022)
28. L. Qiao, W. Zhang, and K. Shi, Anomalous quantum dynamics in lossy nonlocal system, *Chin. Phys. Lett.* 41(12), 120301 (2024)
29. W. T. Xue, Y. M. Hu, F. Song, and Z. Wang, Non-Hermitian edge burst, *Phys. Rev. Lett.* 128(12), 120401 (2022)
30. P. Wen, J. Pi, and G. L. Long, Investigation of a non-Hermitian edge burst with time-dependent perturbation theory, *Phys. Rev. A* 109(2), 022236 (2024)
31. J. Zhu, Y. L. Mao, H. Chen, K. X. Yang, L. Li, B. Yang, Z. D. Li, and J. Fan, Observation of non-Hermitian edge burst effect in one-dimensional photonic quantum walk, *Phys. Rev. Lett.* 132(20), 203801 (2024)
32. L. Xiao, W. T. Xue, F. Song, Y. M. Hu, W. Yi, Z. Wang, and P. Xue, Observation of non-Hermitian edge burst in quantum dynamics, *Phys. Rev. Lett.* 133(7), 070801 (2024)
33. T. Yoshida, T. Mizoguchi, and Y. Hatsugai, Chiral edge modes in evolutionary game theory: A Kagome network

of rock–paper–scissors cycles, *Phys. Rev. E* 104(2), 025003 (2021)

34. T. Yoshida, T. Mizoguchi, and Y. Hatsugai, Non-Hermitian topology in rock–paper–scissors games, *Sci. Rep.* 12(1), 560 (2022)
35. J. Liang, Q. Dai, H. Li, H. Li, and J. Yang, Topological phases in population dynamics with rock–paper–scissors interactions, *Phys. Rev. E* 110(3), 034208 (2024)
36. J. Knebel, P. M. Geiger, and E. Frey, Topological phase transition in coupled rock–paper–scissors cycles, *Phys. Rev. Lett.* 125(25), 258301 (2020)
37. B. C. Kirkup and M. A. Riley, Antibiotic-mediated antagonism leads to a bacterial game of rock–paper–scissors in vivo, *Nature* 428(6981), 412 (2004)
38. D. Semmann, H. J. Krambeck, and M. Milinski, Volunteering leads to rock–paper–scissors dynamics in a public goods game, *Nature* 425(6956), 390 (2003)